Journal of Applied Physics ARTICLE pubs.aip.org/aip/jap

A machine learning approach to reveal microstructures contributing to dislocation clusters in multicrystalline silicon

Cite as: J. Appl. Phys. **137**, 195101 (2025); doi: 10.1063/5.0260424
Submitted: 24 January 2025 · Accepted: 29 April 2025 ·
Published Online: 15 May 2025

Kazuma Torii,[1] Kyoka Hara,[1] Daiki Hatanaka,[1] Takuto Kojima,[2] Kentaro Kutsukake,[1,3,4] Hiroaki Kudo,[5] Ryoji Katsube,[1] and Noritaka Usami[1,3,6,a)]

AFFILIATIONS

[1]Graduate School of Engineering, Nagoya University, Nagoya 464-8603, Japan
[2]National Institute of Advanced Industrial Science and Technology, Tsukuba 305-8561, Japan
[3]Institute of Materials and Systems for Sustainability, Nagoya University, Nagoya 464-8601, Japan
[4]Center of Advanced Intelligence Project, RIKEN, Tokyo 103-0027, Japan
[5]Graduate School of Informatics, Nagoya University, Nagoya 464-8601, Japan
[6]Institutes of Innovation for Future Society, Nagoya University, Nagoya 464-8601, Japan

[a)]**Author to whom correspondence should be addressed:** usami.noritaka.i7@f.mail.nagoya-u.ac.jp

ABSTRACT

We report on our attempts to leverage a machine learning model to investigate the crystallographic features contributing to the dislocation clusters in multicrystalline silicon. The developed model predicts the presence of dislocation clusters at the center of optical images and enables us to obtain their spatial distribution in a wafer by scanning the position for prediction. Information about the crystal orientation distribution was incorporated into the model by using multiple optical images of the textured wafers taken under illumination from various angles of incidence. The area under the curve, an indicator of prediction accuracy, of the optimized model was over 0.99, which is much higher than that of the previous model using optical images taken at a single illumination angle. In addition, the regions of interest in the predictions were evaluated using gradient-based class activation mapping. The results were analyzed using crystal orientation information, and we revealed crystallographic features of the regions surrounding the dislocation clusters. We then proposed a design guideline to produce multicrystalline silicon wafers with a low density of dislocation clusters based on our findings. The prediction of dislocation cluster distribution in the virtual multicrystalline silicon wafer following the guideline indicated that the number of dislocation clusters could be much lower than that in the conventional real multicrystalline silicon wafers. Accordingly, the technique proposed in this study should be effective for rapidly analyzing the relationship between the defects and the microstructure in multicrystalline materials and understanding the physics behind microstructure and defect evolution in the fabrication processes.

I. INTRODUCTION

Multicrystalline materials are widely used in various technical fields including automotive industry, construction and architecture, and electronics due to their ease of mass production. Therefore, deepening our knowledge for enhancing the physical properties of multicrystalline materials is expected to be of social and industrial importance. Controlling crystal defects is an important issue in the development of high-performance multicrystalline materials because they significantly affect the mechanical, electrical, and optical properties. For example, it is well-known that the strength and ductility of a material are affected by the density of the grain boundary[1–4] and that thermal conductivity is reduced by the presence of dislocations, grain boundaries, and impurity atoms.[5,6] A tremendous effort has, therefore, been devoted to manipulate the crystal defects in multicrystalline materials and to develope state-of-the-art materials with excellent properties.

The crystalline defect that is characteristic of multicrystalline materials is grain boundaries, a type of planar defect. There is a large variety of features in multicrystalline materials, such as grain size, grain distribution, relative orientation, and spatial inhomogeneity of physical properties. These features are related to each other and the generation/annihilation of other crystal defects. Designing multicrystalline materials is, therefore, more complex compared to single-crystalline materials. Reflecting this background, there are diverse guiding principles for controlling the microstructure and the defects in multicrystalline materials, especially in the field of metallic materials and ceramics,[7–9] but there is still great room for improvement in understanding how to tailor multicrystalline materials.

The recent development of data science technologies has led to the emergence of a new research field, materials informatics, which aims to advance materials science beyond the limitations of traditional experimental and theoretical science alone.[10–13] Uncovering the physics behind complex microstructures in multicrystalline materials is one of the active research topics in materials informatics.[14–21] The implementation of machine learning techniques has changed the characterization and reconstruction steps in the research of multicrystalline materials;[20] characterization is the evaluation and classification of the microstructure of the materials, and reconstruction is the design of the microstructure appropriate for a particular application. In other words, we can overcome the difficulties behind the development of multicrystalline materials by developing a cutting-edge research framework integrating experimental methods and machine learning techniques.

Multicrystalline silicon is one of the simplest multicrystalline materials that consist of crystal grains with a single crystal structure and a single constituent element. This material is crucial as a light absorber in photovoltaics due to its abundance on Earth and affordability.[22–24] The energy conversion efficiency of solar cells based on multicrystalline silicon depends on the density of dislocation clusters, a type of crystalline defect in which dislocations accumulate at a density of 10^5–10^8 cm^{-2}.[25–28] To improve the energy conversion efficiency, it is essential to reduce the density of dislocation clusters, and understanding the mechanism of their generation is a key issue. Although dislocation cluster formation in multicrystalline silicon has been the focus of extensive research,[28–40] the underlying mechanisms remain unclear, largely due to the complexity of the microstructure and the diversity of grain boundaries. Leveraging machine learning could be effective in tackling this challenge.

One might wonder about the importance of studying multicrystalline silicon, especially given that nearly all newly manufactured solar cells are made from monocrystalline silicon. However, we believe that there is significant value in using simple multicrystalline silicon as a model material. This approach can help develop methodologies to address unresolved issues in complex multicrystalline materials. Moreover, such methodologies could be extended and applied to the research of other materials and various challenges in materials science.

In our previous study, we attempted to elucidate the physical phenomena behind the behavior by constructing a machine learning model that predicts the spatial distribution of dislocation clusters in the multicrystalline wafer and analyzing the internal structure of the model.[41] The model developed in the study used an optical image of a wafer which was textured with alkaline solutions as input data and a photoluminescence (PL) image of the same wafer as teacher data. The optical image contained information about the microstructure because the reflectivity of each grain in the textured wafer depends on the crystal orientation, and the PL image showed the distribution of dislocation clusters. The model successfully predicted the dislocation cluster distribution with the area under the curve of over 0.9, and key regions for decision-making were identified by gradient-based class activation mapping (Grad-CAM). However, the input dataset in the previous study contained limited information on crystal orientation, an important parameter of multicrystalline materials, because the optical images were taken under illumination at a specific angle of the light source. Thus, the model can be further improved whereas it has a high predictive ability in its original state. Also, the statistical analysis of extracted important regions for decision-making and identifying specific mechanisms of generation of dislocation clusters remain an issue.

In this study, we report on the development of an advanced machine learning model that incorporates crystallographic texture information to predict the presence of dislocation clusters in multicrystalline silicon wafers. In addition to developing the machine learning model, we tried to identify important regions for decision-making by Grad-CAM. The regions of interest obtained by Grad-CAM were statistically analyzed to investigate the influence of the crystallographic features on the model's decision and to derive insights into the generation of dislocation clusters.

II. EXPERIMENTAL AND DATA SCIENCE METHODS

A. Collection of optical and PL images

We used two types of images, optical images taken under illumination from a variety of directions and a PL image, to train the machine learning model. The test specimens used for these observations were high-performance multicrystalline silicon wafers produced by Kyocera Corp. The wafer size was 156 mm × 156 mm × 180 μm. Prior to the observation, the wafers were anisotropically etched in an alkaline solution to leave a facet structure consisting of {111} planes on the surface of each crystal grain. The optical images of the wafers after this treatment reflect the crystallographic orientations of the crystal grains as shown in Fig. 1(a) and the reflectance of each crystal grain depends on the direction of the incident light. Consequently, a set of optical images taken under illumination from different directions contains information about the crystallographic texture in the wafer.

For capturing the optical images, we used a custom-made apparatus consisting of a line camera, a telecentric lens, a line light source, and a three-axis moving stage.[42] The parameters for the incident light were elevation angle θ and azimuth angle φ. The textured wafers were also evaluated using a PL imaging system consisting of an InGaAs camera and an excitation light with a wavelength of 940 nm (EPL-100 s, Hamamatsu Photonics, Japan). The PL intensity from the region where dislocation clusters exist is lower than that from the region with a low number of crystal defects, due to non-radiative recombination through defect levels related to the dislocation clusters. As a result, the region with dislocation clusters appears relatively dark in a PL image, as shown in Fig. 1(b). Since

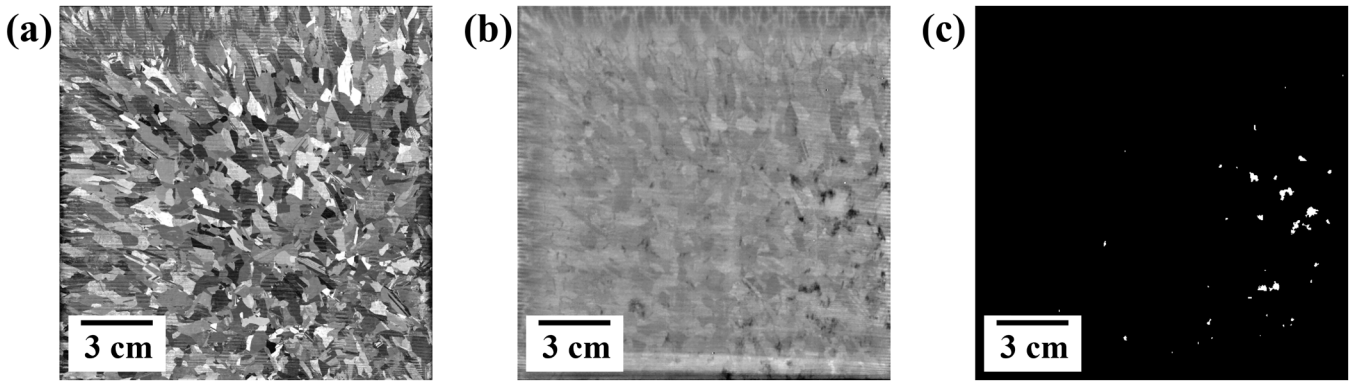

FIG. 1. Examples of the images used to train the machine learning model: (a) optical, (b) PL, and (c) binarized and black/white inverted PL images of a textured multicrystalline silicon wafer.

the contrast induced by dislocation clusters is stronger than other defects such as grain boundaries, the regions rich in dislocation clusters can be clearly observed by binarizing the PL image, as displayed in Fig. 1(c). The spatial resolution was determined by the pixel size of the line camera, which was about 300 μm. Empirically, a dislocation density of $10^5\,\mathrm{cm}^{-2}$, i.e., more than 10 dislocations per pixel, significantly reduces the PL intensity.[43] The presence of the dislocations with a density of more than $10^5\,\mathrm{cm}^{-2}$ can thus be detected by binarizing the PL images.

B. Construction of a dislocation cluster presence prediction model incorporating crystallographic texture information

The brightness of each pixel in the optical image depends on the orientation of the crystal grain and the angle of incident light as mentioned above. In previous studies, we utilized this feature to develop a machine learning model that predicts the crystal orientation by combining the optical images and the crystallographic texture image obtained by the x-ray Laue scanner.[44,45] The basic idea of the present study is the same as these works; it may be possible to incorporate the information on crystal orientation into the machine learning model if we use the optical images taken with various directions of the incident light. Based on the above background, we tried to integrate the optical images taken with different angles of the light source into a single dataset.

To illustrate the idea of this study in detail, we discuss the dependence of the optical images on the direction of the incident light with specific examples. Figure 2(a) shows typical optical images taken at different angles of the incident light source. We focus on three crystal grains annotated in Fig. 2(a). Figure 2(b) shows the relationship between normalized luminance and azimuth angle for the three grains, indicating that the luminance changed depending on the azimuth angle. However, if we compare grains 2 and 3, we can notice that they have similar luminance values in the azimuth range of 0°–25° and at about 140° azimuth. This indicates that it is difficult to distinguish the crystal orientation of crystal grains in the wafer from a single optical image. Also, the probability of this classification error would be reduced by increasing the number of optical images taken from different angles of incident light. Accordingly, we developed machine learning models using various numbers of optical images and will discuss the accuracy of those models in the results and discussion section.

The basic structure of the model is shown in Fig. 3. The model is a convolutional neural network (CNN) consisting of three convolutional layers and one fully connected layer. The convolutional layer extracts important features from the input images. From the extracted features, the discriminator of the neural network makes a label decision. The output value is represented as a score between 0 and 1, where 0 represents the region without dislocation clusters and 1 represents the region with many dislocation clusters. A set of optical images taken at different directions of incident light was used as input data, and a binarized and black/white inverted PL image was used as teacher data. Also, center pixel labels were obtained from the binarized PL image corresponding to the optical images to train the model. The total number of datasets was 38 536, and the datasets were randomly divided into training and validation datasets in a ratio of 80:20. The test data were obtained from a wafer different from the one used for training. To build a model with high accuracy, we searched for the optimal conditions by varying the number and size of optical images.

C. Grad-CAM to visualize the regions of interest in the model

The trained models were analyzed by Grad-CAM.[41,46] In general, the interpretations made by machine learning models are not obvious to us. Grad-CAM is one of the methods to overcome this "black box problem" by providing interpretability to machine learning models.[47–49] Grad-CAM uses the gradient of a pre-trained model to compute feature map weights for class scores and outputs a coarse heat map. This heat map highlights the regions in the input image that are important for evaluating the model. We attempted to extract microstructural information that has a significant influence on the generation of dislocation clusters by analyzing the model using Grad-CAM.

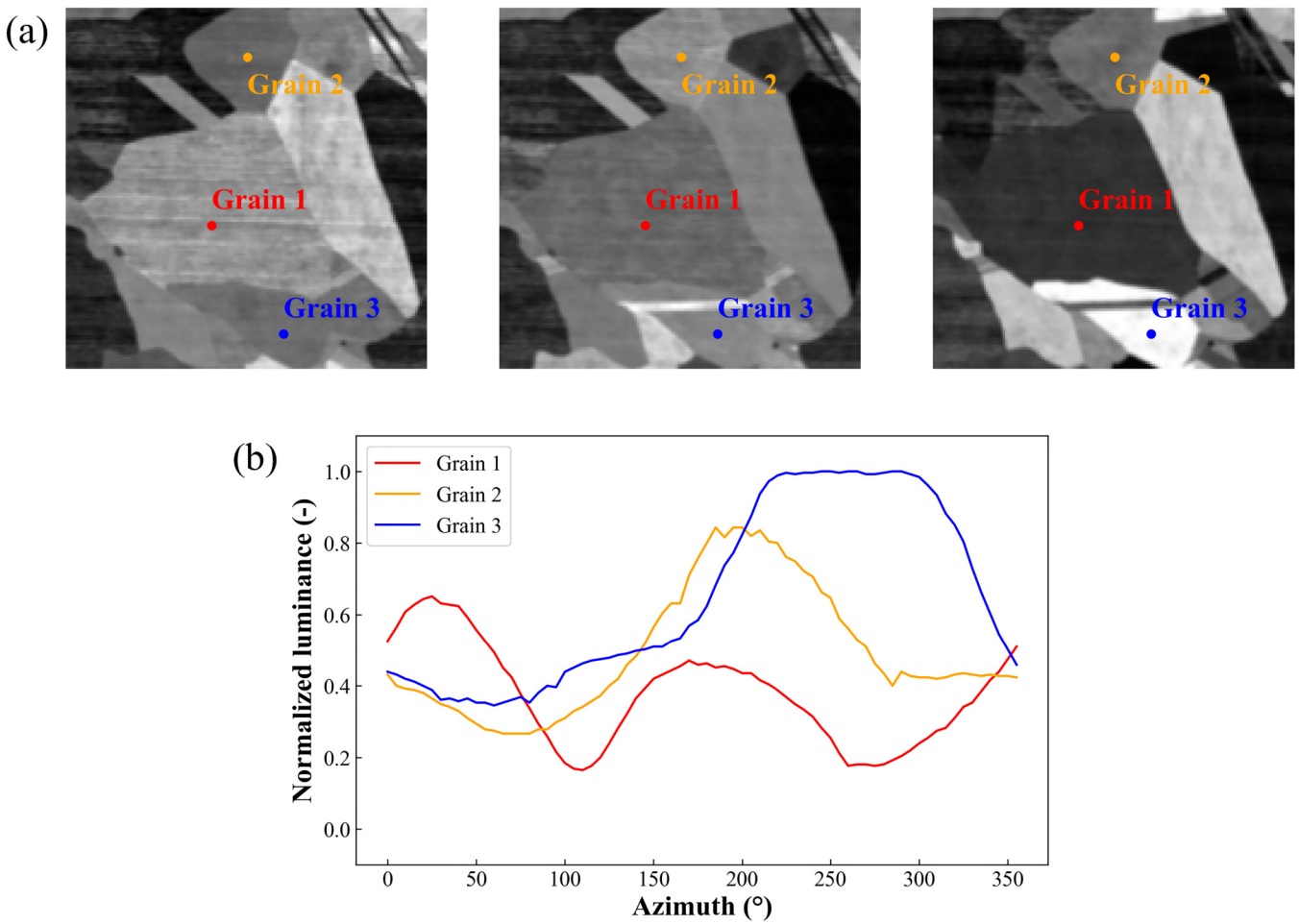

FIG. 2. (a) Typical optical images of a textured multicrystalline silicon wafer taken at different angles of light incidence. (b) Relationship between the azimuth angle of light incidence and the normalized luminance of the three grains in (a).

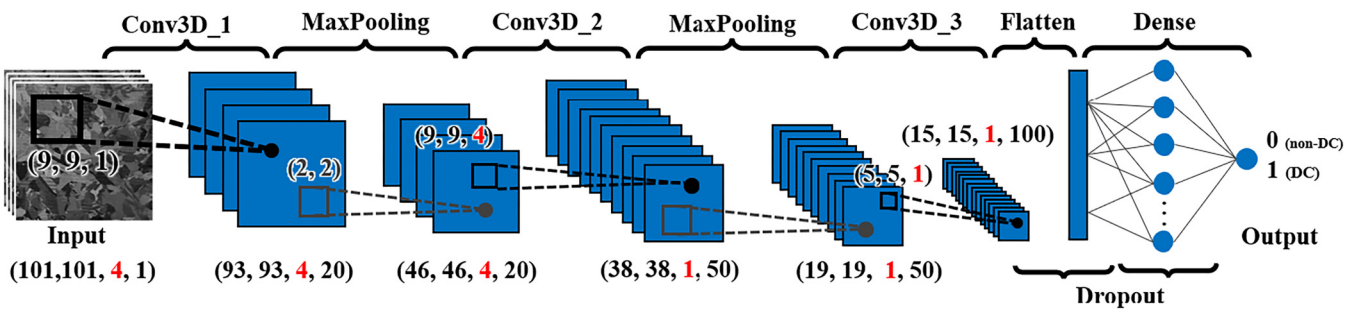

FIG. 3. Schematic illustration of the architecture of the dislocation cluster prediction model.

III. RESULTS AND DISCUSSIONS

A. Training results of a dislocation cluster prediction model that can account for crystal orientation distribution

Figure 4 summarizes the prediction results based on three different sets of input data. In Fig. 4(a), the input data consists only of information on grain shapes, grain distribution, and grain boundaries. In other words, the model in Fig. 4(a) was constructed without information of crystal orientation. To evaluate the models, we used the area under the curve (AUC), which is mainly used in binary classification problems, as an evaluation metric. The AUC value for the model in Fig. 4(a) was 0.51, indicating that the prediction was failed. This result can also be understood by comparing the ground truth and the predicted images, where the spatial distributions of the white pixels are completely different. Optical images taken at a specific direction of the incident light were used as input data to build the model shown in Fig. 4(b), similar to the method employed in the previous study.[41] The AUC value for this model exceeded 0.9, which is significantly larger than that of Fig. 4(a). This result indicates the excellent predictive capability of the model. However, a notable discrepancy was observed between the ground truth and the predicted images shown in Fig. 4(b). Figure 4(c) shows the prediction results of the model proposed in this study. Optical images taken at four different incident light directions were used as input data for developing the model. The AUC value of this model was much higher than the other two models. Furthermore, the positions of the dislocation clusters in the predicted image were consistent with those in the ground truth image. This is thought to be due to the use of multiple optical images, which enabled more accurate identification of crystal orientation within the wafer.

Figure 5 shows the relationship between the number of optical images taken at different directions of the incident light

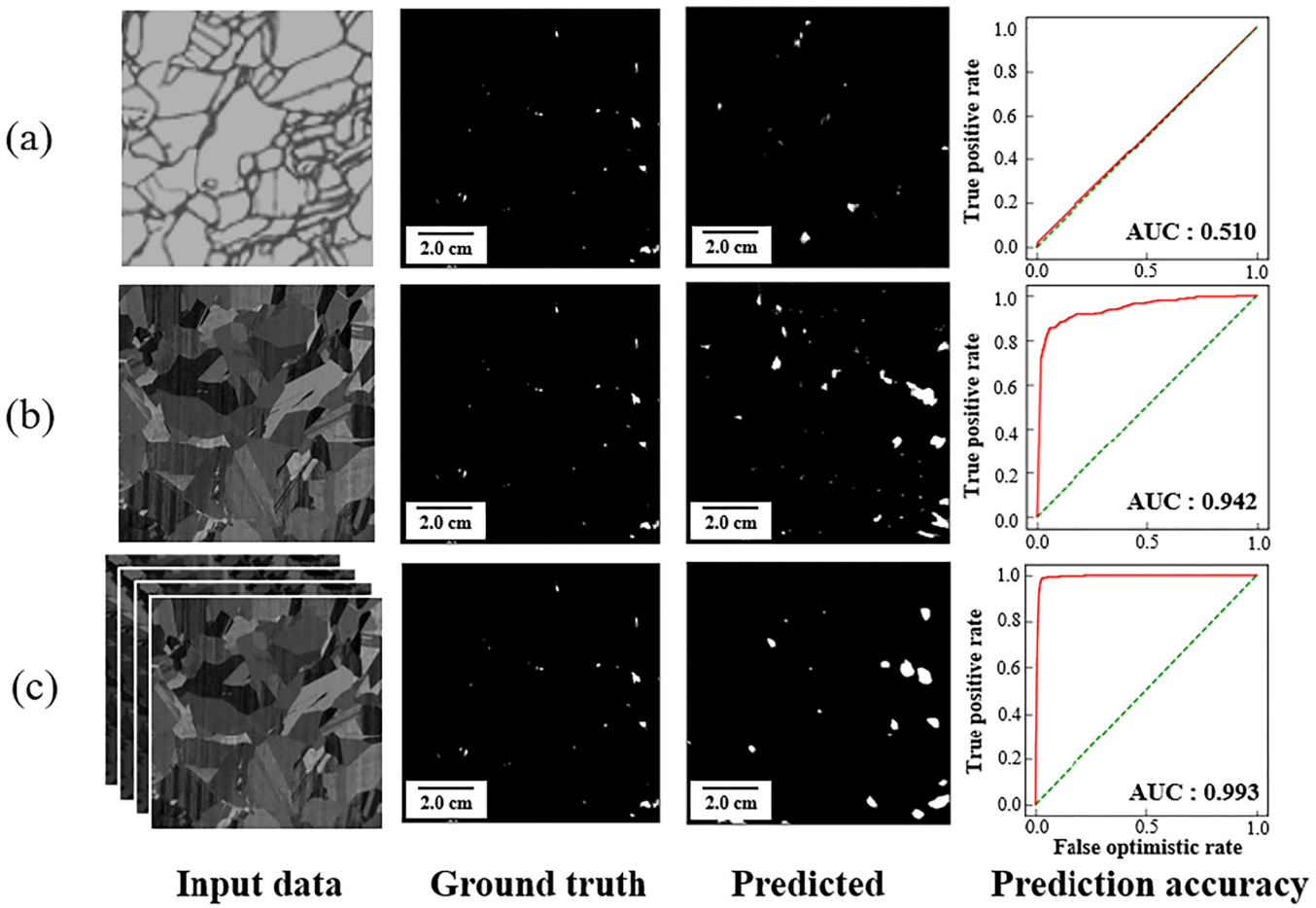

FIG. 4. Input data, ground truth, and predicted images of the spatial distribution of dislocation clusters, and prediction accuracy of the dislocation cluster prediction model with different sets of input data, which were the optical images (a) on which only crystal grain or grain boundary can be distinguished, (b) taken at a specific direction of the incident light, and (c) taken at various directions of the incident light.

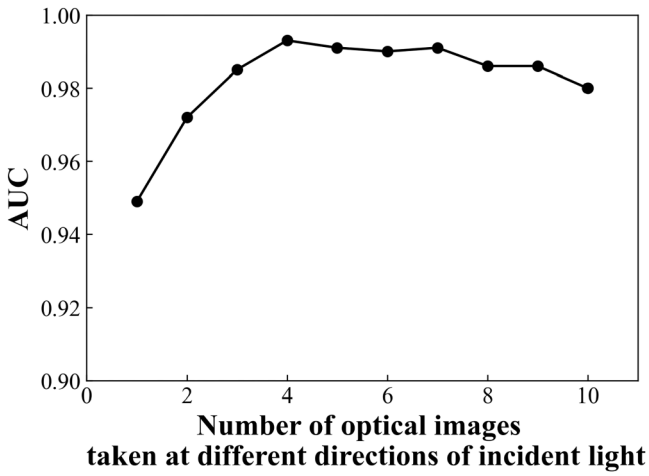

FIG. 5. Relationship between the number of optical images taken from the different directions of incident light in a single dataset and the AUC value of the model.

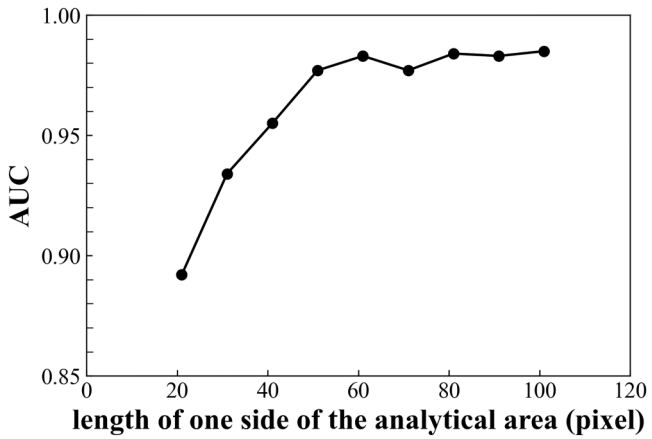

FIG. 6. Relationship between the size of the analytical area and the AUC value of the dislocation cluster prediction model.

in a single dataset and the AUC value, which is an indicator of the accuracy of the model. The AUC value increased monotonically in the range of the number of optical images 1–4, and a slight decrease in the accuracy was observed when the number of images exceeded 4. The increase in AUC value in the small number of images indicates that crystallographic texture information is certainly important for predicting the dislocation cluster distribution. On the other hand, as the number of images increases, the number of parameters to be learned increases, which may require a greater number of training epochs. If the training is not completed effectively, this could lead to a reduction in accuracy. This may be the reason for the slight decrease in AUC value in the number of input images larger than 4. In practice, a significantly high accuracy was achieved with three to four optical images. Therefore, considering both measurement and calculation costs, four optical images are considered to be sufficient.

B. Effect of peripheral microstructure on dislocation cluster generation

We subsequently present the results of our evaluation regarding how peripheral microstructures influence the accuracy of a dislocation cluster prediction model. This analysis was performed by comparing the accuracies of the models constructed using different areas of the optical and PL images for analysis. The results are shown in Fig. 6, where the horizontal axis represents the length of one side of the analytical area used for the prediction of dislocation clusters, and the vertical axis indicates the AUC value of the model. The AUC value increased monotonically with increasing size up to the area of 60×60 pixel^2 (about 3.50 cm^2 in actual size) and remained an almost constant value in the range of the analysis area larger than 60×60 pixel^2. This result suggests that the crystallographic relationship with the nearest and the second nearest neighbor grains may play a critical role in the formation and/or propagation of dislocation clusters in a given crystal grain.

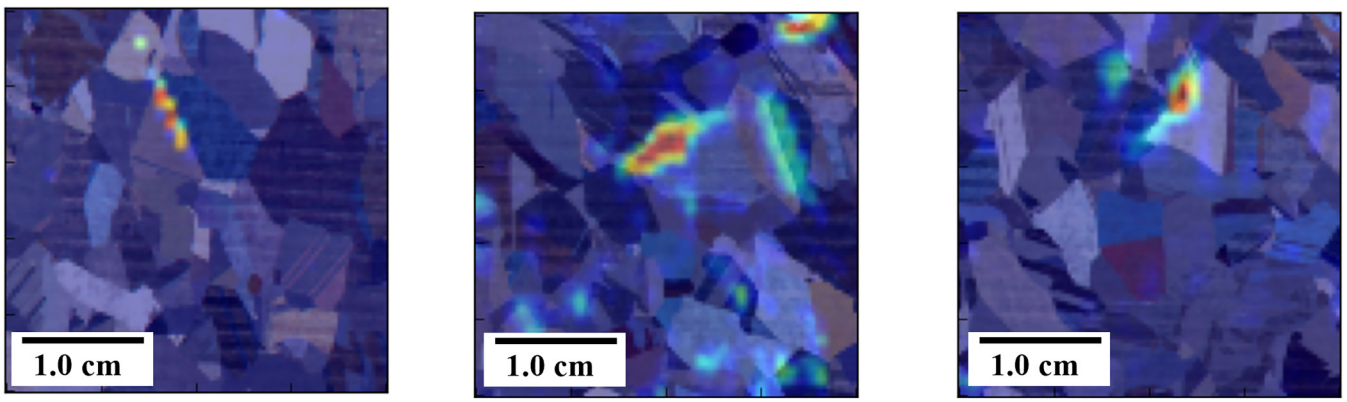

FIG. 7. Examples of the Grad-CAM visualization to visualize the regions of interest in the dislocation cluster prediction model incorporating information of crystallographic texture.

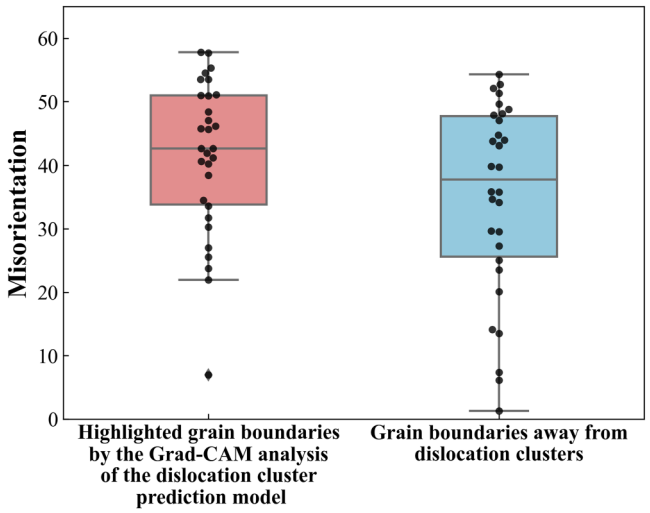

FIG. 8. Distribution of the misorientations at the grain boundaries highlighted by the Grad-CAM analysis and in the area away from the dislocation clusters.

C. Analysis of regions of interest using Grad-CAM

Figure 7 shows examples of the Grad-CAM visualization of the regions of interest in the dislocation cluster prediction model incorporating information on crystallographic texture. The images in Fig. 7 are overlayed ones of the heat map obtained by the Grad-CAM analysis on the optical images of the textured wafers. Also, the Grad-CAM heat maps shown in Fig. 7 are the results for the prediction of the presence or absence of dislocation clusters at the center of the image. Interestingly, the model also focused on the microstructure of the regions outside the image center where no dislocation clusters were present, suggesting that crystal grains and grain boundaries, which are located a short distance away, influence the generation and propagation of dislocation clusters. This is consistent with the discussion in Sec. III B that the microstructural relationships with the surrounding crystal grains may be related to the spatial distribution of dislocation clusters.

To gain further insight into the relationship between the spatial distribution of dislocation clusters and the crystallographic texture, we statistically investigated the crystallographic orientations in the regions of interest identified by the Grad-CAM analysis. The box-and-whisker and scatterplots on the left side of Fig. 8 show the distribution of the difference in crystallographic orientations at the grain boundaries highlighted by the Grad-CAM analysis. Figure 8 also shows the data for the grain boundaries in the regions far away from the dislocation clusters on the right side. The misorientations at the grain boundaries highlighted by the Grad-CAM analysis were mostly distributed in the regions of angles higher than 20°, while those in the regions away from dislocation clusters were widely distributed.

The microstructure around the region of interest in the Grad-CAM was also statistically analyzed. Figure 9(a) summarizes the orientation difference between the grain at the center of the region of interest and its nearest and second nearest neighbors. The results for four different samples are displayed in Fig. 9(a). As a control analysis, the orientation difference between a grain in the region away from dislocation clusters and its nearest and second nearest neighbors was evaluated as shown in Fig. 9(b). The orientation differences shown in Fig. 9(a) were mostly distributed in the regions of angles higher than 20°, similarly to the analysis shown in the left side of Fig. 8. On the contrary, the orientation differences

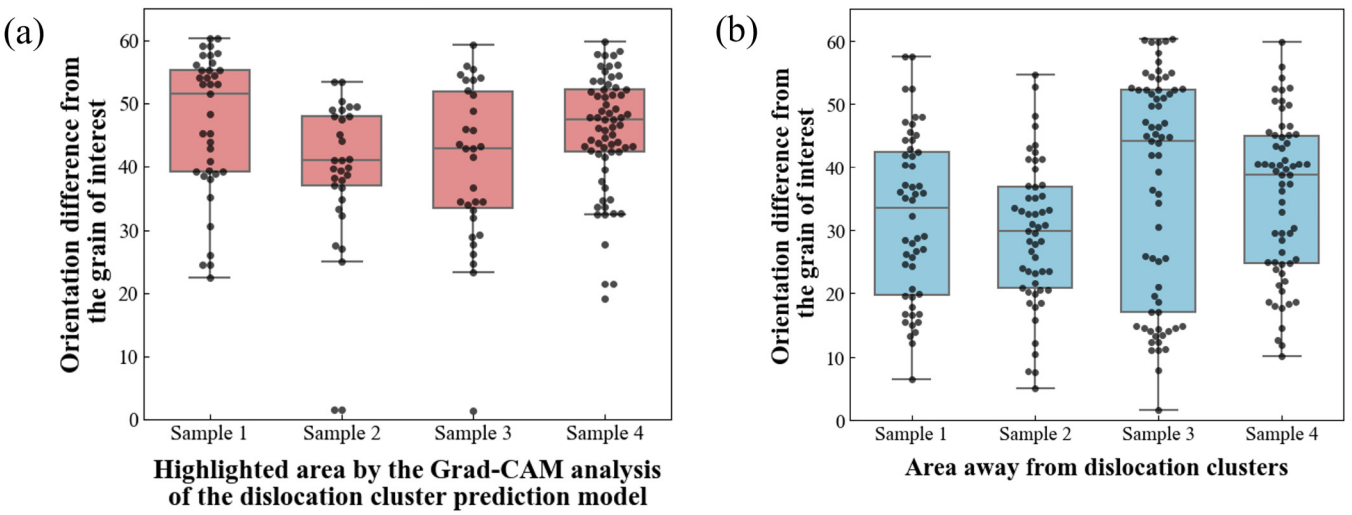

FIG. 9. (a) Distribution of the orientation differences between the grain at the center of the region of interest identified by the Grad-CAM analysis and its nearest and second nearest neighbors. (b) Distribution of the orientation differences between grains in the regions away from dislocation clusters and its nearest and second nearest neighbors.

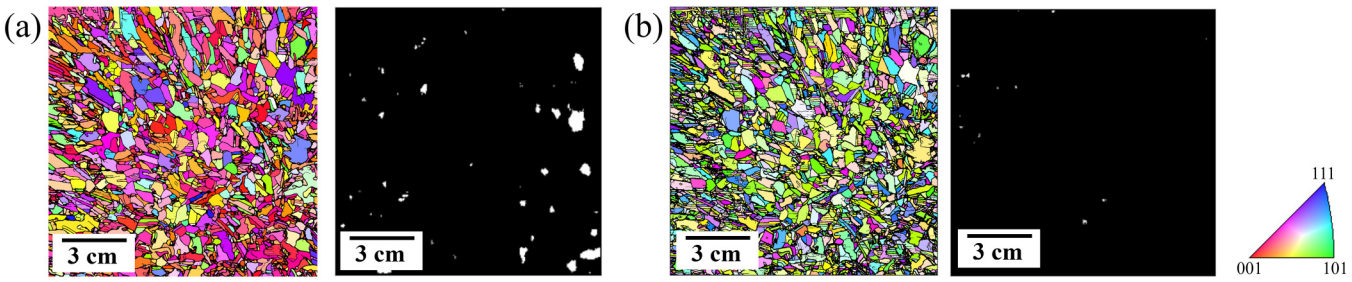

FIG. 10. Crystallographic orientation map and the corresponding predicted dislocation cluster distribution for (a) the real multicrystalline silicon wafer and (b) the virtual multicrystalline silicon wafer generated based on the design guideline proposed in this study.

for other areas were widely dispersed as shown in Fig. 9(b). These results were consistent across the different samples, suggesting that this is a common phenomenon in multicrystalline silicon. Taking the results in this section together, we can conclude that dislocation clusters are surrounded by regions composed of groups of crystal grains that have orientations more than 20° different from other grains. On the contrary, the region away from the dislocation clusters has some pairs of grains with the orientation difference less than 20°.

D. Proposal of guiding principle for high-quality multicrystalline materials

The results so far suggest that there are some areas consisting of grains with relatively large orientation differences around dislocation clusters. In general, the consistency of the atomic arrangement at the grain boundaries deteriorates as the orientation difference between the grains increases, except for the coincidence site lattice grain boundaries. In addition, stress concentration during the solidification and subsequent cooling process would be pronounced around the regions in grains with large orientation differences due to the anisotropy of the physical properties such as linear expansion coefficient, elastic constants, and yield stress. The above properties can cause the generation and propagation of dislocation clusters, and thus we can qualitatively understand the results of the Grad-CAM analysis based on the above discussion.

The insights gained from the Grad-CAM analysis have motivated us to develop a valuable guiding principle for designing multicrystalline materials. According to the results of this study, we considered that multicrystalline silicon consisting of crystal grains oriented within 10° from a certain direction would have a smaller number of dislocation clusters than the existing multicrystalline silicon ingots. To verify this idea, a virtual microstructure of a multicrystalline silicon wafer was generated based on this guideline with reference to the real wafer. The generation procedure is as follows. First, an arbitrary crystal orientation was assigned as a reference to determine the orientations of the grain in the optical image of the real wafer. The brightness profile of the optical images was then replaced for each grain so that the crystal orientation was within 10° of the reference orientation. The microstructure generated in this way has an orientation difference of no more than 20° between any given crystal grains. We validated our idea by predicting dislocation clusters on the optical images of the real wafer and those with modified brightness profiles to reduce the crystallographic orientation difference. Figure 10 shows the crystallographic orientation maps and the results of dislocation cluster prediction for the real and the designed virtual wafers. The number of dislocation clusters in the virtual wafer was obviously smaller than that in the real one. This indicates that multicrystalline silicon wafers with a particularly low density of dislocation clusters, which are attractive for photovoltaic applications, can be produced if we can develop the process to control the microstructure to meet the guideline. To achieve this goal, it is essential to clarify the relationship between the materials process and the resulting microstructures. By integrating simulations based on physical models, experimental data, and machine learning techniques, we may be able to conduct an inverse design of the process starting from the microstructures. This represents an exciting new challenge.

IV. CONCLUSIONS

We have developed an improved machine learning model that predicts the presence of dislocation clusters using optical images taken at multiple angles of light incidence and PL images. The idea of using multiple optical images in a single dataset successfully improved the prediction accuracy of the model, probably because the increased number of optical images resulted in the enrichment of crystallographic information implemented in the model. The Grad-CAM analysis of the constructed model revealed that there was a difference in the crystallographic features of the regions containing dislocation clusters and the other regions. Inspired by these results, we established a guideline for designing high-quality multicrystalline silicon wafers. The effectiveness of the guideline was verified by the virtual generation of the wafers based on the guideline and the prediction of the dislocation cluster distribution, where the density of dislocation clusters in the virtually generated wafer was much lower than those in the real wafers.

The multicrystalline analysis method proposed in this study can be applied to the analysis of other detrimental defects in multicrystalline silicon, such as grain boundaries. A variety of methods are available for the purpose of visualizing the spatial distribution data of carrier recombination rates at grain boundaries, including cathodoluminescence,[50] electron beam induced current,[51–53] and micro-photoluminescence imaging.[54,55] If they could be used as

training data instead of the PL images in this study, we would be able to obtain a prediction model for the spatial distribution of carrier-trapping grain boundaries. The method would also be applicable to various multicrystalline materials if methods for applying the surface structure reflecting the crystallographic orientations and visualization techniques for the spatial distribution of the physical properties of the material of interest are established. There are already well-known methods for the former, such as anisotropic etching or corrosion for diverse materials including metals, covalent crystals, and ionic crystals. The number of established methods applicable to the latter analysis is relatively limited, but recent advances in measurement techniques have been expanding the variety of the properties. Therefore, we believe that the materials informatics approach proposed in this study will contribute to the advancement of various multicrystalline materials.

ACKNOWLEDGMENTS

We acknowledge Dr. Hitoshi Matuo and Dr. Hideyoshi Tanabe of Kyocera Corporation for supplying the multicrystalline silicon wafers used in this study and fruitful discussions. This work was supported by JST, CREST Grant No. JPMJCR17J1, Japan.

AUTHOR DECLARATIONS

Conflict of Interest

The authors have no conflicts to disclose.

Author Contributions

Kazuma Torii: Conceptualization (equal); Data curation (lead); Investigation (lead); Methodology (lead); Validation (lead); Writing – original draft (lead). **Kyoka Hara:** Data curation (supporting); Investigation (supporting); Methodology (supporting). **Daiki Hatanaka:** Data curation (supporting); Investigation (supporting); Methodology (supporting); Validation (supporting). **Takuto Kojima:** Methodology (supporting); Supervision (supporting); Validation (supporting). **Kentaro Kutsukake:** Funding acquisition (supporting); Methodology (supporting); Supervision (supporting). **Hiroaki Kudo:** Funding acquisition (supporting); Methodology (supporting); Supervision (supporting). **Ryoji Katsube:** Methodology (supporting); Supervision (supporting); Writing – review & editing (equal). **Noritaka Usami:** Conceptualization (equal); Funding acquisition (lead); Supervision (lead); Writing – review & editing (equal).

DATA AVAILABILITY

The data that support the findings of this study are available from the corresponding author upon reasonable request.

REFERENCES

[1]K. S. Kumar, H. Van Swygenhoven, and S. Suresh, "Mechanical behavior of nanocrystalline metals and alloys," Acta Mater. **51**(19), 5743–5774 (2003).
[2]M. A. Meyers, A. Mishra, and D. J. Benson, "Mechanical properties of nanocrystalline materials," Prog. Mater. Sci. **51**(4), 427–556 (2006).
[3]L. Lu, X. Chen, X. Huang, and K. Lu, "Revealing the maximum strength in nanotwinned copper," Science **323**(5914), 607–610 (2009).
[4]K. Lu, L. Lu, and S. Suresh, "Strengthening materials by engineering coherent internal boundaries at the nanoscale," Science **324**(5925), 349–352 (2009).
[5]S. Il Kim, K. H. Lee, H. A. Mun, H. S. Kim, S. W. Hwang, J. W. Roh, D. J. Yang, W. H. Shin, X. S. Li, Y. H. Lee, G. J. Snyder, and S. W. Kim, "Dense dislocation arrays embedded in grain boundaries for high-performance bulk thermoelectrics," Science **348**(6230), 109–114 (2015).
[6]B. Poudel, Q. Hao, Y. Ma, Y. Lan, A. Minnich, B. Yu, X. Yan, D. Wang, A. Muto, D. Vashaee, X. Chen, J. Liu, M. S. Dresselhaus, G. Chen, and Z. Ren, "High-thermoelectric performance of nanostructured bismuth antimony telluride bulk alloys," Science **320**(5876), 634–638 (2008).
[7]T. Koseki and G. Thewlis, "Overview inclusion assisted microstructure control in C–Mn and low alloy steel welds," Mater. Sci. Technol. **21**(8), 867–879 (2005).
[8]Y.-W. Kim, "Intermetallic alloys based on gamma titanium aluminide," JOM **41**(7), 24–30 (1989).
[9]I. Weiss and S. L. Semiatin, "Thermomechanical processing of alpha titanium alloys—An overview," Mater. Sci. Eng. A **263**(2), 243–256 (1999).
[10]S. Hong, C. H. Liow, J. M. Yuk, H. R. Byon, Y. Yang, E. Cho, J. Yeom, G. Park, H. Kang, S. Kim, Y. Shim, M. Na, C. Jeong, G. Hwang, H. Kim, H. Kim, S. Eom, S. Cho, H. Jun, Y. Lee, A. Baucour, K. Bang, M. Kim, S. Yun, J. Ryu, Y. Han, A. Jetybayeva, P.-P. Choi, J. C. Agar, S. V. Kalinin, P. W. Voorhees, P. Littlewood, and H. M. Lee, "Reducing time to discovery: Materials and molecular modeling, imaging, informatics, and integration," ACS Nano **15**(3), 3971–3995 (2021).
[11]J. M. Rickman, H. M. Chan, M. P. Harmer, J. A. Smeltzer, C. J. Marvel, A. Roy, and G. Balasubramanian, "Materials informatics for the screening of multi-principal elements and high-entropy alloys," Nat. Commun. **10**(1), 1–10 (2019).
[12]A. Agrawal and A. Choudhary, "Perspective: Materials informatics and big data: Realization of the 'fourth paradigm' of science in materials science," APL Mater. **4**(5), 053208 (2016).
[13]F. Oba and Y. Kumagai, "Design and exploration of semiconductors from first principles: A review of recent advances," Appl. Phys. Express **11**(6), 060101 (2018).
[14]M. Mińkowski and L. Laurson, "Predicting elastic and plastic properties of small iron polycrystals by machine learning," Sci. Rep. **13**(1), 13977 (2023).
[15]M. O. Buzzy, A. E. Robertson, and S. R. Kalidindi, "Statistically conditioned polycrystal generation using denoising diffusion models," Acta Mater. **267**, 119746 (2024).
[16]M. Dai, M. F. Demirel, X. Liu, Y. Liang, and J. M. Hu, "Graph neural network for predicting the effective properties of polycrystalline materials: A comprehensive analysis," Comput. Mater. Sci. **230**, 112461 (2023).
[17]J. C. Stinville, J. M. Hestroffer, M. A. Charpagne, A. T. Polonsky, M. P. Echlin, C. J. Torbet, V. Valle, K. E. Nygren, M. P. Miller, O. Klaas, A. Loghin, I. J. Beyerlein, and T. M. Pollock, "Multi-modal dataset of a polycrystalline metallic material: 3D microstructure and deformation," Sci. Data **9**(1), 1–16 (2022).
[18]A. Rovinelli, M. D. Sangid, H. Proudhon, and W. Ludwig, "Using machine learning and a data-driven approach to identify the small fatigue crack driving force in polycrystalline materials," npj Comput. Mater. **4**(1), 35 (2018).
[19]S. Noguchi, S. Aihara, and J. Inoue, "Microstructure estimation by combining deep learning and phase transformation model," ISIJ Int. **64**(1), 142–153 (2024).
[20]R. Bostanabad, Y. Zhang, X. Li, T. Kearney, L. C. Brinson, D. W. Apley, W. K. Liu, and W. Chen, "Computational microstructure characterization and reconstruction: Review of the state-of-the-art techniques," Prog. Mater. Sci. **95**, 1–41 (2018).
[21]Z.-L. Wang and Y. Adachi, "Property prediction and properties-to-microstructure inverse analysis of steels by a machine-learning approach," Mater. Sci. Eng. A **744**, 661–670 (2019).
[22]Y. M. Yang, A. Yu, B. Hsu, W. C. Hsu, A. Yang, and C. W. Lan, "Development of high-performance multicrystalline silicon for photovoltaic industry," Prog. Photovoltaics: Res. Appl. **23**(3), 340–351 (2015).
[23]S. Pizzini, "Towards solar grade silicon: Challenges and benefits for low cost photovoltaics," Sol. Energy Mater. Sol. Cells **94**(9), 1528–1533 (2010).

[24]M. E. Meral and F. Dinçer, "A review of the factors affecting operation and efficiency of photovoltaic based electricity generation systems," Renew. Sustain. Energy Rev. **15**(5), 2176–2184 (2011).
[25]H. J. Möller, C. Funke, M. Rinio, and S. Scholz, "Multicrystalline silicon for solar cells," Thin Solid Films **487**(2), 179–187 (2005).
[26]S. Castellanos, K. E. Ekstrom, A. Autruffe, M. A. Jensen, A. E. Morishige, J. Hofstetter, P. Yen, B. Lai, G. Stokkan, C. Del Canizo, and T. Buonassisi, "High-performance and traditional multicrystalline silicon: Comparing gettering responses and lifetime-limiting defects," IEEE J. Photovoltaics **6**(3), 632–640 (2016).
[27]B. Sopori, P. Rupnowski, V. Mehta, V. Budhraja, S. Johnston, N. Call, H. Mountinho, M. Al-Jassim, A. Shaikh, M. Seacrist, and D. Carlson, "Performance limitations of mc-Si solar cells caused by defect clusters," ECS Trans. **18**(1), 1049–1058 (2009).
[28]V. Kveder, M. Kittler, and W. Schröter, "Recombination activity of contaminated dislocations in silicon: A model describing electron-beam-induced current contrast behavior," Phys. Rev. B **63**(11), 115208 (2001).
[29]B. Ryningen, G. Stokkan, M. Kivambe, T. Ervik, and O. Lohne, "Growth of dislocation clusters during directional solidification of multicrystalline silicon ingots," Acta Mater. **59**(20), 7703–7710 (2011).
[30]D. Oriwol, M. Trempa, L. Sylla, and H. S. Leipner, "Investigation of dislocation cluster evolution during directional solidification of multicrystalline silicon," J. Cryst. Growth **463**, 1–9 (2017).
[31]I. Takahashi, N. Usami, K. Kutsukake, G. Stokkan, K. Morishita, and K. Nakajima, "Generation mechanism of dislocations during directional solidification of multicrystalline silicon using artificially designed seed," J. Cryst. Growth **312**(7), 897–901 (2010).
[32]N. Zhou, X. Sui, X. He, S. Huang, and L. Zhou, "Nucleation of self-growth dislocations on growth front during the solidification process of silicon," J. Appl. Phys. **125**(15), 155108 (2019).
[33]M. Trempa, I. Kupka, C. Kranert, T. Lehmann, C. Reimann, and J. Friedrich, "Evolution of grain structure and recombination active dislocations in extraordinary tall conventional and high performance multi-crystalline silicon ingots," J. Cryst. Growth **459**, 67–75 (2017).
[34]G. Stokkan, Y. Hu, Ø. Mjøs, and M. Juel, "Study of evolution of dislocation clusters in high performance multicrystalline silicon," Sol. Energy Mater. Sol. Cells **130**, 679–685 (2014).
[35]A. Autruffe, V. Stenhjem Hagen, L. Arnberg, and M. Di Sabatino, "Dislocation generation at near-coincidence site lattice grain boundaries during silicon directional solidification," J. Cryst. Growth **411**, 12–18 (2015).
[36]S. Nakano, X. J. Chen, B. Gao, and K. Kakimoto, "Numerical analysis of cooling rate dependence on dislocation density in multicrystalline silicon for solar cells," J. Cryst. Growth **318**(1), 280–282 (2011).
[37]I. Takahashi, S. Joonwichien, S. Matsushima, and N. Usami, "Relationship between dislocation density and contact angle of dendrite crystals in practical size silicon ingot," J. Appl. Phys. **117**(9), 095701 (2015).
[38]G. Stokkan, A. Song, and B. Ryningen, "Investigation of the grain boundary character and dislocation density of different types of high performance multicrystalline silicon," Crystals **8**(9), 341 (2018).
[39]Y. Ohno, K. Tajima, K. Kutsukake, and N. Usami, "Generation of dislocation clusters at triple junctions of random angle grain boundaries during cast growth of silicon ingots," Appl. Phys. Express **13**(10), 105505 (2020).
[40]K. Yamakoshi, Y. Ohno, K. Kutsukake, T. Kojima, T. Yokoi, H. Yoshida, H. Tanaka, X. Liu, H. Kudo, and N. Usami, "Multicrystalline informatics applied to multicrystalline silicon for unraveling the microscopic root cause of dislocation generation," Adv. Mater. **36**(8), 2308599 (2024).
[41]K. Hara, T. Kojima, K. Kutsukake, H. Kudo, and N. Usami, "3D CNN and grad-CAM based visualization for predicting generation of dislocation clusters in multicrystalline silicon," APL Mach. Learn. **1**(3), 036106 (2023).
[42]N. Usami, K. Kutsukake, T. Kojima, H. Kudo, T. Yokoi, and Y. Ohno, "Multicrystalline informatics: A methodology to advance materials science by unraveling complex phenomena," Sci. Technol. Adv. Mater. **25**(1), 2396272 (2024).
[43]Y. Hayama, T. Matsumoto, T. Muramatsu, K. Kutsukake, H. Kudo, and N. Usami, "3D visualization and analysis of dislocation clusters in multicrystalline silicon ingot by approach of data science," Sol. Energy Mater. Sol. Cells **189**, 239–244 (2019).
[44]K. Hara, T. Kojima, K. Kutsukake, H. Kudo, and N. Usami, "A machine learning-based prediction of crystal orientations for multicrystalline materials," APL Mach. Learn. **1**(2), 026113 (2023).
[45]H. Kato, S. Kamibeppu, T. Kojima, K. Kutsukake, T. Yamamoto, H. Kudo, Y. Takeuchi, and N. Usami, "Crystallographic orientation prediction of multicrystalline silicon substrate using machine learning," IEICE Tech. Rep. **119**, 81–84 (2020).
[46]R. R. Selvaraju, M. Cogswell, A. Das, R. Vedantam, D. Parikh, and D. Batra, "Grad-CAM: Visual explanations from deep networks via gradient-based localization," Int. J. Comput. Vision **128**, 336–359 (2020).
[47]R. Guidotti, A. Monreale, S. Ruggieri, F. Turini, D. Pedreschi, and F. Giannotti, "A survey of methods for explaining black box models," ACM Comput. Surv. **51**(5), 1–42 (2018).
[48]A. Barredo Arrieta, N. Díaz-Rodríguez, J. Del Ser, A. Bennetot, S. Tabik, A. Barbado, S. Garcia, S. Gil-Lopez, D. Molina, R. Benjamins, R. Chatila, and F. Herrera, "Explainable artificial intelligence (XAI): Concepts, taxonomies, opportunities and challenges toward responsible AI," Inf. Fusion **58**, 82–115 (2020).
[49]J. Schmidt, M. R. G. Marques, S. Botti, and M. A. L. Marques, "Recent advances and applications of machine learning in solid-state materials science," npj Comput. Mater. **5**(1), 83 (2019).
[50]W. Lee, J. Chen, B. Chen, J. Chang, and T. Sekiguchi, "Cathodoluminescence study of dislocation-related luminescence from small-angle grain boundaries in multicrystalline silicon," Appl. Phys. Lett. **94**(11), 112103 (2009).
[51]J. Chen, T. Sekiguchi, D. Yang, F. Yin, K. Kido, and S. Tsurekawa, "Electron-beam-induced current study of grain boundaries in multicrystalline silicon," J. Appl. Phys. **96**(10), 5490–5495 (2004).
[52]A. Stoffers, O. Cojocaru-Mirédin, W. Seifert, S. Zaefferer, S. Riepe, and D. Raabe, "Grain boundary segregation in multicrystalline silicon: Correlative characterization by EBSD, EBIC, and atom probe tomography," Prog. Photovoltaics: Res. Appl. **23**(12), 1742–1753 (2015).
[53]J. Chen, T. Sekiguchi, S. Nara, and D. Yang, "The characterization of high quality multicrystalline silicon by the electron beam induced current method," J. Phys.: Condens. Matter **16**(2), S211–S216 (2004).
[54]F. Schindler, J. Giesecke, B. Michl, J. Schön, P. Krenckel, S. Riepe, W. Warta, and M. C. Schubert, "Material limits of multicrystalline silicon from state-of-the-art photoluminescence imaging techniques," Prog. Photovoltaics: Res. Appl. **25**(7), 499–508 (2017).
[55]T. Mchedlidze, W. Seifert, M. Kittler, A. T. Blumenau, B. Birkmann, T. Mono, and M. Müller, "Capability of photoluminescence for characterization of multicrystalline silicon," J. Appl. Phys. **111**(7), 073504 (2012).